Desalination and Water Treatment
www.deswater.com

doi: 10.1080/19443994.2015.1043953

57 (2016) 11195–11210
May

Taylor & Francis
Taylor & Francis Group

Removal of Pb(II) ion from aqueous solution by graphene oxide and functionalized graphene oxide-thiol: effect of cysteamine concentration on the bonding constant

Mohammad Yari[a,*], Mehdi Norouzi[b], Amir Hossein Mahvi[c], Mostafa Rajabi[d], Ali Yari[e], Omid Moradi[e], Inderjeet Tyagi[f], Vinod Kumar Gupta[f,g,h]

[a]*Department of Chemistry, Eslamshahr Branch, Islamic Azad University, Eslamshahr, Iran, emails: dr.m.yari1966@gmail.com, yari@iiau.ac.ir (M. Yari)*
[b]*Department of Virology, School of Genetics, School of Public Health, Tehran University of Medical Sciences, Tehran, Iran*
[c]*School of Public Health and Institute for Environmental Research, Tehran University of Medical Sciences, Tehran, Iran*
[d]*Department of Chemistry, Arak Branch, Islamic Azad University, Arak, Iran*
[e]*Department of Chemistry, Shahre-Qods Branch, Islamic Azad University, Tehran, Iran, emails: o.moradi@shahryaiu.ac.ir, moradi.omid@gmail.com (O. Moradi)*
[f]*Department of Chemistry, Indian Institute of Technology Roorkee, Roorkee 247667, India, Tel. +91 1332285801; Fax: +91 1332273560; emails: vinodfcy@iitr.ac.in, vinodfcy@gmail.com (V.K. Gupta)*
[g]*Center for Environment and Water, The Research Institute, King Fahd University of Petroleum & Minerals, Dhahran 31261, Saudi Arabia*
[h]*Department of Applied Chemistry, University of Johannesburg, Johannesburg, South Africa*

Received 6 December 2014; Accepted 9 April 2015

ABSTRACT

Efficient adsorbent graphene oxide (GO) and its derivative, i.e., thiol-functionalized graphene oxide (GO-SH), was used for the removal of noxious Pb(II) ion from the aqueous phase. Different amounts, i.e., 60, 80, and 100 mg of cysteamine, were used as functionalizing agent to functionalize the GO with thiol group; hence, three different nanocomposites, i.e., GO-SH_1, GO-SH_2, and GO-SH_3 were prepared from the different amount of the cysteamine. The developed nanocomposites were characterized using various analytical techniques such as Fourier transform infrared spectroscopy, scanning electron microscopy, and X-ray diffraction analysis. The whole removal and adsorption process was well illustrated and investigated. The impact of influential factors including initial concentration, pH, contact time, temperature, and concentrations cysteamine on the adsorption properties of Pb(II) from aqueous solution was well elucidated and optimized. The obtained equilibrium results were inserted in various adsorption isotherm models such as Langmuir (liner types I, II, III, and IV), Freundlich, Temkin, Helsey, and Dubinin-Radushkevich isotherms, it was found that the Langmuir (type I) model demonstrated was well fitted and in good agreement with the maximum adsorption of Pb(II) ion from aqueous solution. Thermodynamic functions, such as ΔG°, ΔH°, and ΔS° were calculated and it reveals that the adsorption of Pb(II) ion on all the surfaces was spontaneous and endothermic in nature.

*Corresponding author.

Keywords: Graphene oxide; Cysteamine; Thiol functionalization; Pb(II) ion; Adsorption

1. Introduction

Existence of heavy metal ions in the aquatic streams is nowadays of great concern for the rapidly developing ecosystem and biome. Contamination and pollution caused due to the presence of heavy metals has received keen attention because of their detrimental toxic effects on the human health and biotic organisms [1]. Effluents of industrial wastewaters consist of many toxic heavy metals ions such as lead, mercury, chromium, nickel, cadmium, and zinc ions which lead to severe toxic effects on soil as well as aquatic ecosystem [2]. One of the most venomous heavy metals reported was lead ion which was present in the environment in micro level; nowadays it is reported as the major noxious pollutant present in the aquatic ecosystem. Even trace levels of lead could be harmful to biotic organisms, all lead ions compounds were considered as cumulative toxicants [3]. The enrichment and bioavailability of Pb(II) ion by plants and crops lead to the noticeable transfer Pb(II) ion from ecosystem to the prevailing food chains [4]. The concentration of Pb(II) ion in wastewater was found much higher than the permissible limits (0.05 mg/L) specified by environment protection agency [1]. Adsorption being a most economical and efficient method, has been widely applied for the removal of heavy metal ion from wastewater [5]. A number of materials, including activated carbon (AC), zeolites, carbon nanotube sheets [6], chitosan/poly (acrylic acid) magnetic composite [7], chitosan [8], chitosan activated carbon composite [9], carbon nanotubes (CNTs) [10], and thiol-functionalized cellulosic biomass [11] were used as adsorbents for the efficient removal of toxic impurities from the wastewater.

Recently, the application of nanomaterial in wastewater treatment has attracted significant and keen attentions of the scientific world; due to the unique properties of the nanomaterial, i.e., large surface areas and more activated functionalized sites [12], it is considered as the efficient adsorbent nowadays. Graphene and its derivatives were lately emerged as carbonaceous nanomaterials, their characteristic structures and electronic properties make them interact forcefully with organic and inorganic impurity molecules, via non-covalent forces, such as hydrogen bonding, π–π stacking, electrostatic forces, vander waals forces, and hydrophobic interactions [13]. However, the excessive use of graphene on a large scale was limited by the prevailing difficulties of separation and regeneration of graphene. Graphene-based adsorbents with extremely high efficiency, low cost, convenient regeneration as well as easy separation were highly desired [14]. Graphene basically is a 2D carbon nanomaterial with single layer of sp^2-hybridized carbon atoms arranged in six-membered rings [15,16].

In the present work, the rapid removal of Pb(II) ion by developed adsorbent, i.e., GO, GO-SH_1, GO-SH_2, and GO-SH_3 were well investigated and studied. Various analytical techniques like Fourier transform infrared spectroscopy (FT-IR) and scanning electron microscopy (SEM) were used for the characterization the surface GO as nanocomposite. The purpose of this present study was as follows: (i) To specify the effect of cysteamine concentrations to adsorb Pb(II) ions on GO, GO-SH_1, GO-SH_2, and GO-SH_3 as adsorbents; (ii) To measure the adsorption isotherm parameters of Langmuir (linear types: I, II, III, and IV), Freundlich, Temkin, Helsey, and Dubinin–Radushkevich; (iii) To derive the thermodynamic parameters, i.e., ΔG°, ΔH°, and ΔS° during adsorption; (iv) To determine the effect of cysteamine concentrations on the bonding constant.

2. Experimental

2.1. Materials

Graphene Oxide (GO) (4 mg/mL, Water Dispersion) from graphene, N,N-dimethyl formamide (DMF, 99.9%), 1-ethyl-(3-3-dimethylaminopropyl) carbodiimide (EDC, 99%), N-hydroxy succinimide (NHS, 99.9%), and cysteamine hydrochloride ([NH_2 $(CH2)_2$ SH·HCl], (99.9%) were purchased from Sigma-Aldrich Company, Germany. The aqueous solution of Pb(II) ion (25 mg/L) was prepared by using $Pb(NO_3)_2$ (molecular weight, 331.20 g/mol) which was supplied by Merck, Germany (maximum purity available) and was used as received. The pH of the working solution was carefully adjusted using dilute HCl or NaOH solution.

2.2. Synthesis of GO, GO-SH_1, GO-SH_2, and GO-SH_3 surfaces as adsorbents

GO powders were further derivatized to thiol-functionalized GO by reaction with cysteamine hydrochloride of different concentrations, i.e., 60, 80, and 100 mg in ethanol (40 mL) in the presence of a coupling agent, EDC (48 mg) and NHS (30 mg), at

60°C for 48 h, as result of this three different nanocomposites were prepared, i.e., GO-SH_1, GO-SH_2, and GO-SH_3 as adsorbents. All GO surfaces possessing thiol group with different concentrations (GO-SHs) were purified by filtering in a (0.2 μm) membrane followed by washing with abundant amounts of ethanol and water (1:1 (v/v)) and then dried at 80°C for 24 h. These developed GO-SHs were used as adsorbents for the removal of Pb(II) ion from aqueous solution.

2.3. Adsorption studies

Stock solutions of 1,000 mg L^{-1} lead Pb(II) ion in distilled de-ionized water was prepared from the salt precursors $Pb(NO3)_2$ [17], the working concentrations were prepared by the further dilution of the stock solution with the distilled water. All removal presses was carried out using fixed concentration, i.e., 20 mL lead ion aqueous solutions maintained at appropriate pH, along with addition of 20 mg of GO, GO-SH_1, GO-SH_2, and GO-SH_3, respectively. The bottles of solutions were placed in an ultrasonic bath, which was operated at pre-defined temperatures and time. Using a recalculating water system for maintaining the temperature in an ultrasonic bath, the lead ions and adsorbents samples were filtered through a 0.2-μm cellulose membrane filter and the suspensions containing of Pb(II), GO, GO-SH_1, GO-SH_2, and GO-SH_3 were centrifuged at 4,500 rpm for 4 min, the concentrations of remaining Pb(II) ion was analyzed using the atomic absorbance spectrophotometry AAS (Perkin–Elmer AAnalyst 700) and measured (±0.01%) [18]. Then, the amount of the Pb(II) ion removal by the GO-SHs was determined by the difference between the initial and residual concentration of Pb(II) ion solution. The removal capacity of Pb(II) on GO-SHs was calculated using Eq. (1) [19]:

$$q_e = \left(\frac{C_0 - C_e}{W}\right) \times V \quad (1)$$

where q_e is the amount of Pb(II) ion taken up by the adsorbent (mg g^{-1}), C_0 is the initial Pb(II) ion concentration (mg L^{-1}), C_e is the Pb(II) ion concentration (mg L^{-1}) after the adsorption process, W is adsorbent mass (g), and V is the volume of the Pb(II) ion solution (L) [19]. Adsorptions time curve for removal of Pb(II) ion by GO, GO-SH_1, GO-SH_2, and GO-SH_3 as adsorbents in is shown in Fig. 1.

To estimate the fitness of isotherm equations to the experimental data, the chi-square statistic (X^2) was used to measure the isotherm constants. X^2 can be defined as [20]:

$$X^2 = \sum_i^N \frac{\left(q_{e,exp} - q_{e,cal}\right)^2}{q_{e,cal}} \quad (2)$$

3. Results and discussion

3.1. Characterization of GO and GO-SH as adsorbents

The general characterization of the synthesized GO-SH_1, GO-SH_2, and GO-SH_3 adsorbents was carried out using analytical techniques such as SEM and FT-IR, the typical morphological characteristics of samples were examined by SEM (JEOL JSM-5600 Digital Scanning Electron Microscope), as shown in Fig. 2. The microstructures of surfaces of GO were observed by SEM as adsorbents and are shown in Fig. 2.

The functional groups present on the adsorbent surface were characterized using an FT-IR spectroscopy (BOMEM, made in 85 Canada, 100 spectra accumulation, 2 m^{-1} resolution) Spectra were acquired in the 4,000–400 cm^{-1} range (Fig. 3). The FT-IR spectra of GO can be seen in Fig. 3(A). All the samples have strong band at ~3,430 cm^{-1}, which corresponds to characteristic bands of (–OH) [21]. The band around 1,730 cm^{-1} for GO related of the carboxylic acid Group (COO^-) [22], and the band at ~1,620 cm^{-1} for GO assigned to (C=C) skeletal stretching. In addition, the band of ~1,070 cm^{-1} for GO corresponds to the (C–O) vibration of various oxygen-containing group. In Fig. 3(B), reveals the FT-IR spectra of GO functionalized with thiol group using different concentration of cysteamine on GO surface. Evidence of the carboxyl peak at 1,705 cm^{-1}, hydroxyl peak at near 3,405 cm^{-1} was observed. When GO was mixed with cysteamine in the presence of DMF as solvent and EDC and NHS as chemical initiator reaction, the GO functionalized with thiol group GO-SH was derivatized (Fig. 2). The response between the GO–COOH and cysteamine was confirmed by the appearance of a strong aliphatic C–H stretching vibration at ~2,890 cm^{-1}, and an amide (I) band at 1,620 cm^{-1} in this figure. Presence of a peak at ~1,620 cm^{-1} was strongly suggesting that indicated amide group on the surface of GO.

3.2. Effect of contact time and mechanism on the adsorption of Pb(II) ion

For the determination of contact time on the adsorption of Pb(II) ions on GO, GO-SH_1, GO-SH_2, and GO-SH_3 surfaces, the developed adsorbents were contacted with Pb(II) ion solution having

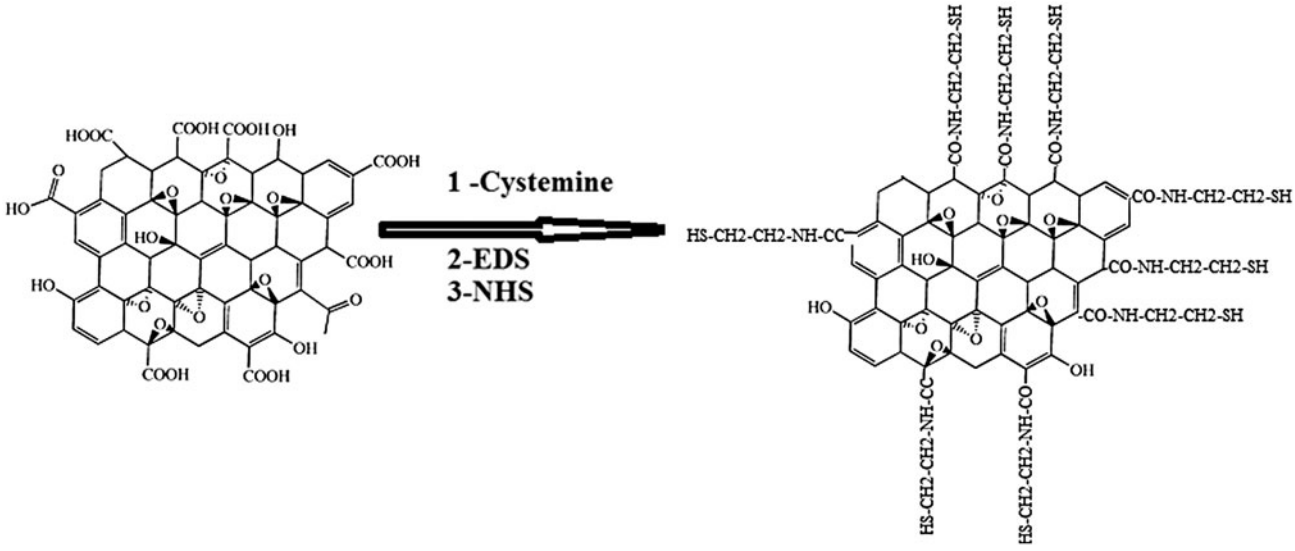

Fig. 1. Schema of functionalized GO–COOH in order to synthesis G–CO–NH–CH_2–CH_2–SH (G-SH) surfaces as new

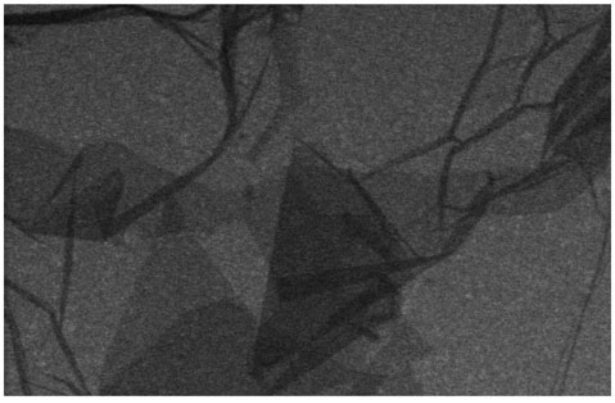

Fig. 2. SEM image of surface of GO.

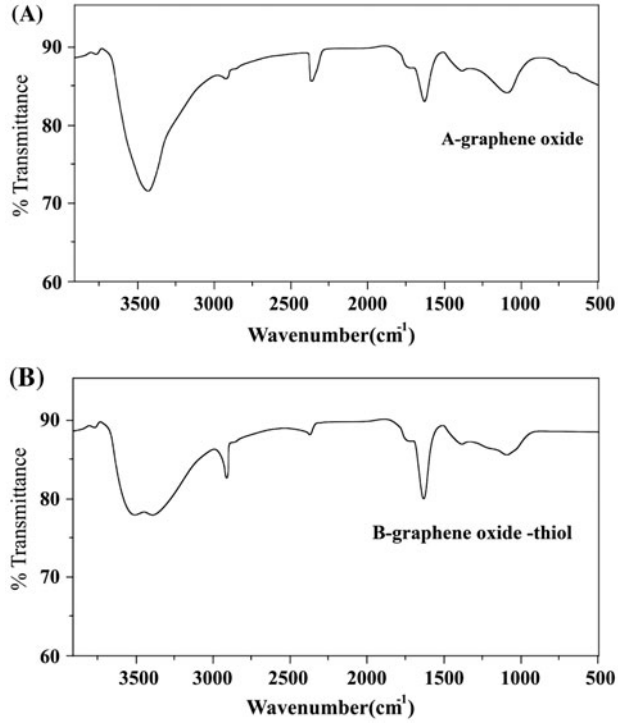

Fig. 3. FTIR spectra of GO (A) and GO-SH (B).

25 mg/L of concentration, in pH 6 and $T = 298$ K. The concentration of Pb(II) ion on the surfaces was analyzed by AAS. Fig. 4 curve shows the amount of Pb(II) ion adsorbed by GO, GO-SH_1, GO-SH_2, and GO-SH_3 surfaces as a function of contact time.

Also, Fig. 4 reveals that the adsorption process occurred during the first 50 min was rapid, which was later followed by a slower adsorption rate. The equilibration time for this process was achieved within 80 min. Hence, these preliminary kinetic experiments strongly suggested that the adsorption of Pb(II) ions was a two-step process; initially, there was a rapid adsorption of metal ions to the surface of adsorbents and latterly it was followed by possible slow intracellular diffusion in the interior of the adsorbents [23–25].

For Pb(II) ion, the equilibration time adsorption on GO, GO-SH_1, GO-SH_2, and GO-SH_3 surfaces was 60 min at initial concentrations of 25 mg/L. The amounts of Pb(II) ion were adsorbed on GO, GO-SH_1,

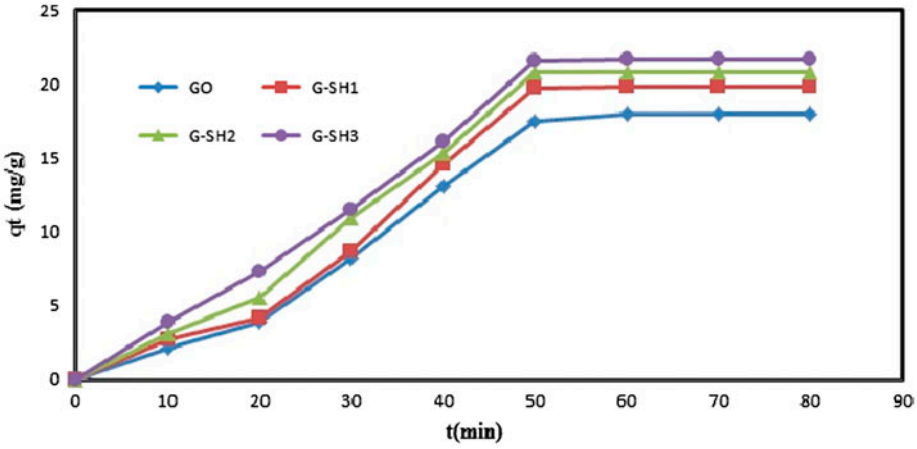

Fig. 4. Effect of contact time on the removal of the Pb(II) ions using GO, GO-SH_1, GO-SH_2, and GO-SH_3 adsorbents, initial concentration: 25 mg/L; adsorbent dosage: 20 mg; and *T:* 298 K. pH 6.

GO-SH_2, and GO-SH_3 surfaces at equilibrium were 18, 19.8, 20.8, and 21.7 (mg/g), respectively. Therefore, this time was chosen as the optimum contact time for all further experiments.

3.3. *Effect of pH*

To determine the impact of pH on the adsorption of Pb(II) ion adsorption using GO and GO-SH_1, GO-SH_2, and GO-SH_3 as adsorbents, a curve of pH (2–9) is shown in Fig. 5. It was found that for all adsorbents, the removal was found to increase with increasing pH up to 7; afterward, it decreased when moved to the alkaline pH. Additionally, increasing in pH of solution from 2 to 7, initial Pb(II) ions concentration: 25 mg L^{-1}, mass of adsorbents: 20 mg, the temperature: 298 K, and contact time: 60 min leads to increase in the amount of lead ion adsorption by GO, GO-SH_1, GO-SH_2, and GO-SH_3 surface as adsorbents, (q_e) from 13.9 to 19.2 (mg/g), 16.4 to 20.7 (mg/g), 16.9 to 21.3 (mg/g), and 17.1 to 22.5 (mg/g) for GO, GO-SH_1, GO-SH_2, and GO-SH_3 surface, respectively [24]. Afterward, the increase in pH from 7 to 9 leads to the decrease in the amount of lead ion adsorbed by GO, GO-SH_1, GO-SH_2, and GO-SH_3 surfaces, (q_e) from 19.2 to 18.8 (mg/g), 20.7 to 19.8 (mg/g), 21.3 to 20.3 (mg/g), and 22.5 to 21.5 (mg/g) for GO, GO-SH_1, GO-SH_2, and GO-SH_3 surfaces, respectively.

In all samples, there has been competitive adsorption among hydronium ions (H_3O^+) and Pb(II) ions. In low pH values, hydronium ion was adsorbed more in comparison with Pb(II), whereas hydronium ions have large concentration and high tendencies to be adsorbed on the surfaces [25]. As the value of pH

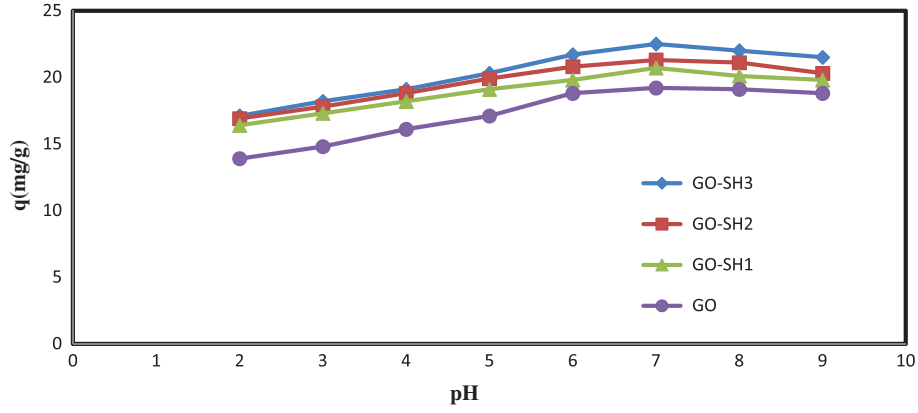

Fig. 5. Effect of pH on the adsorption of Pb(II) ions on GO, GO-SH_1, GO-SH_2, and GO-SH_3 surfaces. Conditions: C_0: 25 mg L^{-1} of Pb(II) solution; mass of adsorbents: 20 mg; the temperature: 298 K; and time: 60 min.

increases, (H_3O^+) ion concentration in the solution decreases which results in more adsorption of Pb(II) ions from the solution [26–28]. Thus, considerable increase in the amount of adsorption and rapid removal of Pb(II) ion takes place in the physiological range of pH, i.e., 6–7. At higher pH values, the precipitation of Pb(II) takes place on GO, GO-SH_1, GO-SH_2, and GO-SH_3 surfaces and the adsorbents were deteriorated with the reposition of lead ion on adsorbents surfaces [28]. So from further experiments, pH 6 was found to be the optimum pH of solution. Like values of optimum pH were reported by some earlier studies for metal ion removal by different adsorbents [25,27]. The results demonstrated that in pH 6, adsorption of Pb(II) ion on GO, GO-SH_1, GO-SH_2, and GO-SH_3 surfaces was greatest.

3.4. Effect of adsorbent composition

In aqueous solution during the contact of adsorbent molecules with another phase (solid, liquid, or a gas) which is insolvable, the ions tend to huddle in the interface of two phases. This orientation has a high affluence at different natural and technological processes [25]. When a solid surface of adsorbent comes in contact with the noxious metal ion, then the rapid removal of ions takes place from the aqueous solution [29]. One of the most important factors in adsorption processes was adsorbent composition. The affluence of adsorbent composition on the removal capacity of Pb (II) ion by GO, GO-SH_1, GO-SH_2, and GO-SH_3 surfaces is shown in Fig. 6. At this part, GO (0 mg of cysteamine), GO-SH_1 (60 mg of cysteamine), GO-SH_2 (80 mg of cysteamine), and GO-SH_3 (100 mg of cysteamine) surfaces were prepared and placed in the aqueous solutions containing 25 mg L^{-1} of Pb(II) ion at pH 6, temperature was 298 K, and the contact time was 60 min. The deionized water for prepared the Pb (II) ions and adsorbents solutions. With increasing cysteamine concentration from 0 to 100 mg, at GO, GO-SH_1, GO-SH_2, and GO-SH_3 surfaces adsorption of Pb(II) ion from aqueous solution increased. With the change of adsorbent composition and increment in the cysteamine concentration, the removal capacity of the developed adsorbent increases owing to increase of the active sites on the surfaces of GO, GO-SH_1, GO-SH_2, and GO-SH_3 surfaces which lead to the infiltration of the Pb(II) ion at the adsorbent site more comfortably. As well as, marvelous interaction increased between Pb(II) ion and GO, GO-SH_1, GO-SH_2, and GO-SH_3 surfaces. The increase of cysteamine concentration, increased the adsorption capacity of Pb (II) ion, which lead to the increased number of functional groups (S–H) and (N–H) on the adsorbent surfaces. (Fig. 1)

3.5. Effect of temperature on the adsorption of Pb(II) ion

One of the factors affecting the adsorption capacity is temperature. Fig. 7 reveals the effect of the temperature on the adsorption capacity of Pb(II) ion on GO, GO-SH_1, GO-SH_2, and GO-SH_3 surfaces at temperature ranging from 288 to 318 K, this process was carried out at contact time 60 min and pH 6. Adsorption capacity of Pb(II) ion on GO, GO-SH_1, GO-SH_2, and GO-SH_3 surfaces increased with increase in the

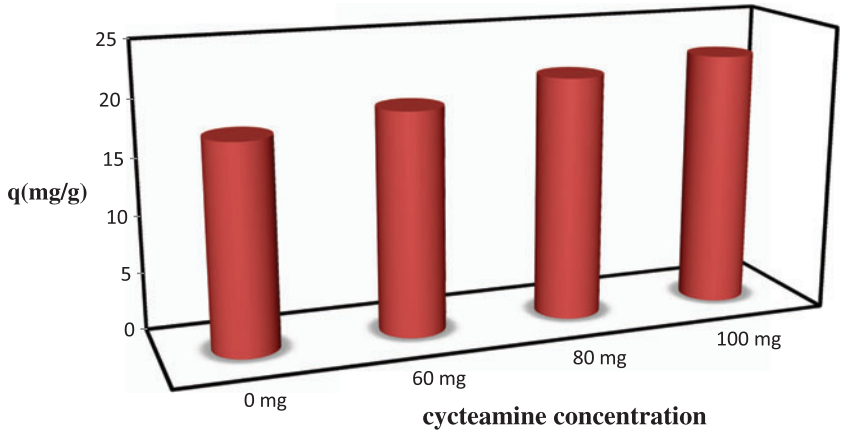

Fig. 6. Effect of cysteamine concentration on the adsorption of Pb(II) ions on adsorbents. 0 mg of cysteamine concentration (GO), 60 mg of cysteamine concentration (GO-SH_1), 80 mg of cysteamine concentration (GO-SH_2) and 100 mg of cysteamine concentration (GO-SH_3). Conditions: C_0: 25 mg L^{-1} of Pb(II) solution; mass of adsorbents: 20 mg; the temperature: 298 K; and time: 60 min and pH 6.

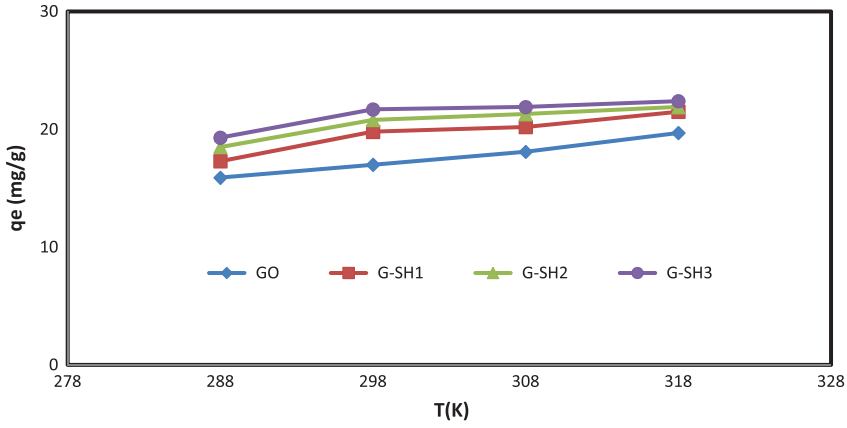

Fig. 7. Effect of temperature on the removal of the Pb(II) ions using GO, GO-SH_1, GO-SH_2, and GO-SH_3 adsorbents, initial concentration: 25 mg/L; adsorbent dosage: 20 mg; time: 60 min; and pH 6.

temperature of surrounding. It was seen that when the temperature increased from 288 to 308 K, the adsorption capacity was increased from 15.9 to 19.7 mg/g for GO surface, 17.3 to 21.5 mg/g for GO-SH_1 surface, 18.5 to 21.9 mg/g for GO-SH_2 surface, and 19.3 to 22.4 mg/g for GO-SH_3 surface in the equilibrium time. This upshot may corroborate the endothermic nature of Pb(II) ion adsorption on GO, GO-SH_1, GO-SH_2, and GO-SH_3 adsorbents, which was consistent with the thermodynamic parameters in this study. Moreover, the positive value of ΔH° was confirmed by the endothermic nature of adsorption and further supported by the increasing adsorption capacity with the increase in temperature for all surfaces as adsorbents (GO GO-SH_1, GO-SH_2, and GO-SH_3) (Table 5). Higher temperature therefore better favored for the adsorption. Furthermore, it may be an indication of ion-exchange adsorption mechanism. While the positive value of ΔS° of all surfaces as adsorbents, may be attributed to the increasing randomness during the adsorption process [29], and further indicated that interactions of Pb(II) with active groups may lead ion to structural changes of adsorbents [30].

3.6. Effect of initial Pb(II) ion concentration on the removal

The removal of Pb(II) ion was performed using various initial concentrations from 5, 15, 25, 35, and 45 mg/g at pH 6, at temperature 298 K and 60 min. As shown in Fig. 8, with increase in the initial concentrations of Pb(II) from 5 to 45 mg/g, the adsorption capacity was increased from 3.1 to 34.1 mg/g, 3.7 to 36.6 mg/g, 3.9 to 38.2 mg/g, and 4.1 to 40.7 mg/g for GO, GO-SH_1, GO-SH_2, and GO-SH_3 adsorbents, respectively. These results perchance be described by the fact that, at the optimum pH, the surface of GO, GO-SH_1, GO-SH_2, and GO-SH_3 adsorbents would be as well as besieged by (H_3O^+) ions which elevate ions interactions with binding sites of the surface GO, GO-SH_1, GO-SH_2, and GO-SH_3 adsorbents or via higher attractive forces [25].

3.7. Adsorption Isotherm

The removal capacity of Pb(II) ion by GO, GO-SH_1, GO-SH_2, and GO-SH_3 adsorbents, simulated by the four linear types of Langmuir [31], the Freundlich [32], the Temkin [33], the Halsey [34], and the Dubinin-Radushkevich (D-R) [35] isotherm models. Also, the models were evaluated by the adjusted determination factor (R^2adj); in addition, to estimate the fitness of isotherm equations to the experimental data, the chi-square statistic (X^2) was used to measure the isotherm constants [36].

3.7.1. Langmuir isotherm model

The Langmuir isotherm model is one of the most prevalent isotherm models which was widely used in the equilibrium study. It is observed that the Langmuir isotherms can be linearized to at least four different types. The four types of Langmuir isotherm model can be expressed as [31]:

$$\text{Type (I)}: \frac{C_e}{q_e} = \frac{1}{KQ_m} + \frac{C_e}{Q_m} \tag{3}$$

$$\text{Type (II)}: \frac{1}{q_e} = \frac{1}{Q_m} + \frac{1}{KQ_mC_e} \tag{4}$$

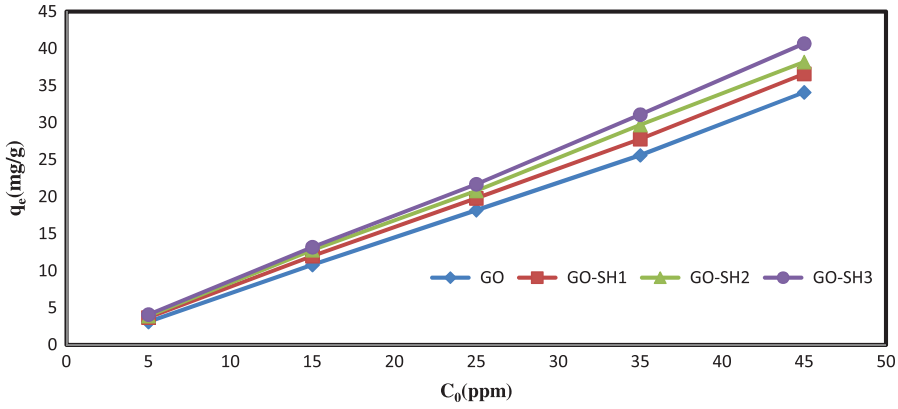

Fig. 8. Effect of initial Pb(II) concentration on the adsorption by GO, GO-SH_1, GO-SH_2, and GO-SH_3 adsorbents. Initial concentration 5–45 mg/L; adsorbent dosage: 20 mg; time: 60 min; and pH 6.

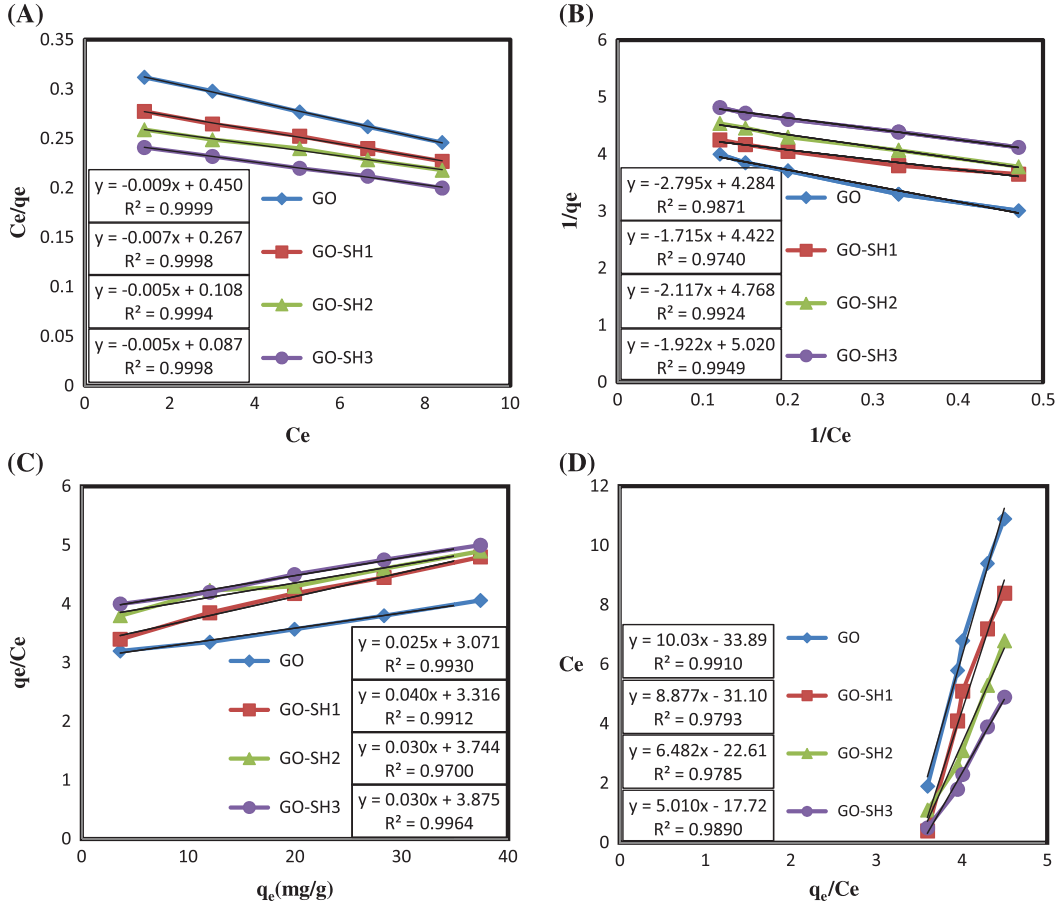

Fig. 9. Langmuir isotherm of Pb(II) ions on GO, GO-SH_1, GO-SH_2, and GO-SH_3 surface (A) type 1 Langmuir, (B) type 2 Langmuir, (C) type 3 Langmuir, and (D) type 4 Langmuir. Initial concentration 5–45 mg/L; adsorbents dosage: 20 mg; time: 60 min; and pH 6.

Table 1
Langmuir isotherm parameters and X^2 parameter for adsorption of Pb(II) ions on GO and GO-SHs surfaces. Initial concentration: 5–45 mg/L; adsorbent dosage: 20 mg; time: 60 min; and pH 6

Isotherm	Equation	Parameters	Adsorbent			
			GO	G-SH_1	G-SH_2	G-SH_3
Langmuir 1	$\frac{C_e}{q_e} = \frac{1}{KQ_m} + \frac{C_e}{Q_m}$	Q_m (mg g^{-1})	111.1	142.8	200	200
		K_1 (L mg^{-1})	0.020	0.026	0.046	0.057
		X^2	0.09	0.05	0.45	0.52
		R^2	0.9999	0.9998	0.9994	0.9998
Langmuir 2	$\frac{1}{q_e} = \frac{1}{Q_m} + \frac{1}{KQ_mC_e}$	Q_m (mg g^{-1})	0.233	0.226	0.210	0.199
		K_2 (L mg^{-1})	1.535	2.580	2.249	2.615
		X^2	2.65	2.98	2.70	2.49
		R^2	0.9870	0.9740	0.9920	0.9940
Langmuir 3	$q_e = Q_m - \frac{q_e}{KC_e}$	Q_m (mg g^{-1})	3.004	3.367	3.688	3.897
		K_3 (L mg^{-1})	35.71	26.31	31.25	34.48
		X^2	2.01	2.11	2.07	2.18
		R^2	0.9990	0.9980	0.9970	0.9990
Langmuir 4	$\frac{q_e}{C_e} = KQ_m - Kq_e$	Q_m (mg g^{-1})	3.39	3.50	3.49	3.54
		K_4 (L mg^{-1})	10.03	8.877	6.482	5.010
		X^2	1.98	2.58	2.69	2.99
		R^2	0.9900	0.9790	0.9780	0.9890

$$\text{Type (III)}: \frac{1}{q_e} = \frac{1}{Q_m} + \frac{1}{KQ_mC_e} \quad (5)$$

$$\text{Type (IV)}: \frac{q_e}{C_e} = KQ_m - Kq_e \quad (6)$$

where Q_m (mg g^{-1}) and K (L/mg) are Langmuir constants corresponds to removal capacity and energy of adsorption. Curve of four types of Langmuir isotherm models shown in Fig. 9 and value of parameters as shown in Table 1.

Comparing the correlation coefficient values (R-values which obtained from the coefficient of determination (R^2) values) and the chi-square statistic (X^2) of used isotherm models. The results demonstrated that the adsorption capacity of Pb(II) ion on GO, GO-SH_1, GO-SH_2, and GO-SH_3 surfaces as adsorbents, Langmuir isotherm model (type I) appeared to fit the isotherm better than Freundlich, Temkin, Helsey, and Dubinin-Radushkevich isotherm models. The maximum Pb(II) ion adsorption capacities (Q_m) obtained from the Langmuir model (type I) were 111.1, 142.8, 200, and 203 mg g^{-1} GO, GO-SH_1, GO-SH_2, and GO-SH_3 as adsorbents, respectively.

Also, dimensionless separation factor (R_L) corresponds the removal of Pb(II) ion by GO and GO-SHs surfaces was calculated use Eq. (7) [31]:

$$R_L = \frac{1}{1 + KC_0} \quad (7)$$

If $R_L > 1$, unfavorable; $R_L = 1$, linear; $0 < R_L < 1$, favorable; $R_L = 0$, irreversible [31]. In this experiment, the R_L lies between 0.63–0.94, 0.46−0.88, 0.33–0.81 and 0.28−0.78 corresponds to GO, GO-SH_1, GO-SH_2, and GO-SH_3 surface, respectively, the values of R_L are shown in Table 2.

3.7.2. Freundlich isotherm model

The Freundlich [32] isotherm is derived by assuming a heterogeneous surface with a no uniform distribution of the heat of sorption over the surface. It can be linearly expressed as follows:

$$q_e = K_F C_e^{1/n} \quad (8)$$

where K_F and n are the Freundlich parameters related to adsorption capacity and adsorption intensity, respectively. If the value of $1/n$ was lower than 1, it indicates a normal Langmuir isotherm; otherwise, it indicates toward the cooperative adsorption. The Freundlich constants can be obtained from the plot of $\log q_e$ vs. $\log C_e$ [32], as shown in Fig. 10(A) and Table 3.

3.7.3. Temkin isotherm model

Temkin and Pyzhev considered the effects of some indirect adsorbent–adsorbate interaction on adsorption isotherms and suggested that the heat of adsorption of

Table 2
Langmuir isotherm dimensionless separation factor (R_L) for adsorption of Pb(II) ions on GO and GO-SHs surfaces. Initial concentration: 5–45 mg/L; adsorbent dosage: 20 mg; time: 60 min; and pH 6

Isotherm	Parameter	Adsorbent			
		GO	GO-SH1	GO-SH2	GO-SH3
Langmuir 1	R_{L1}	0.6314–0.9390	0.4612–0.8854	0.3261–0.8131	0.2818–0.7793
Langmuir 2	R_{L2}	0.0084–0.0710	0.0098–0.0817	0.0085–0.0719	0.0146–0.1152
Langmuir 3	R_{L3}	0.0006–0.0058	0.0007–0.0064	0.0008–0.0075	0.0006–0.0056
Langmuir 4	R_{L4}	0.0044–0.0384	0.0034–0.0358	0.0025–0.2237	0.0022–0.0196

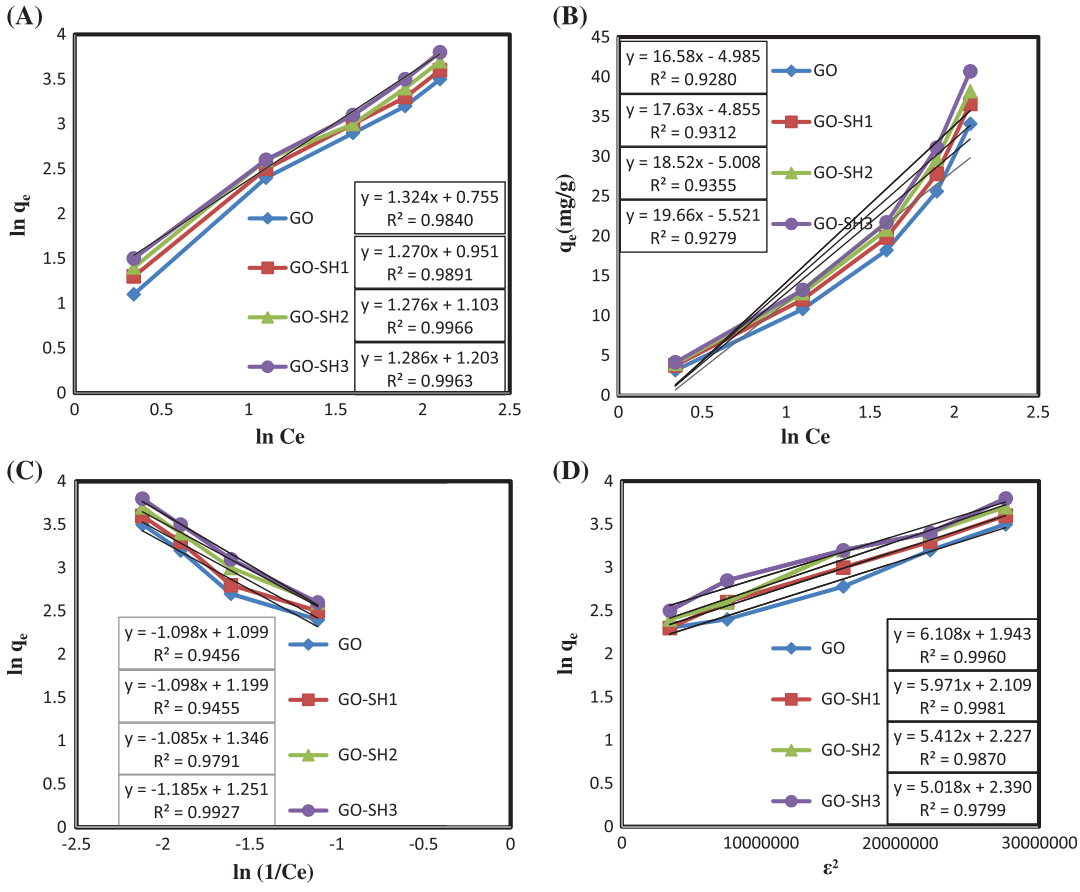

Fig. 10. (A) Freundlich adsorption isotherm of Pb(II) ions using GO, GO-SH_1, GO-SH_2, and GO-SH_3 adsorbents. (B) Temkin adsorption isotherm of Pb(II) ions using GO, GO-SH_1, GO-SH_2, and GO-SH_3 adsorbents. (C) Halsey adsorption isotherm of Pb(II) ions using GO, GO-SH_1, GO-SH_2, and GO-SH_3 adsorbent. (D) Dubinin-Radushkevich (D-R) adsorption isotherm of Pb(II) ions using GO, GO-SH_1, GO-SH_2, and GO-SH_3 adsorbent. Initial concentration: 5–45 mg/L; adsorbent dosage: 20 mg; time: 60 min and pH 6.

all the molecules in the layer would linearly decrease with coverage because of these interactions [33]. The Temkin isotherm has been applied in the following form:

$$q_e = B \ln A + B \ln C_e \quad (9)$$

where B is the Temkin constant related to adsorption heat and A (l/mg) is the Temkin parameter related to the equilibrium binding energy. The Temkin constants can be derived from the plot of q_e vs. ln C_e (as shown in Fig. 10(B) and Table 3).

Table 3
The Freundlich, Temkin, Dubinin-Radushkevich, and Halsey, isotherm parameters and X^2 parameter for adsorption of Pb (II) ions on GO and GO-SHs surfaces. Initial concentration 5–45 mg/L; adsorbent dosage: 20 mg; time: 60 min; and pH 7

Isotherm	Equation	Parameters	Adsorbent			
			Go	G-SH_1	G-SH_2	G-SH_3
Freundlich	$q_e = K_F C_e^{1/n}$	K_F	0.281	0.050	0.098	0.185
		$1/n$	0.755	0.787	0.784	0.778
		X^2	37.9	37.5	36.8	36.9
		R^2	0.9840	0.9891	0.9966	0.9963
Temkin	$q_e = B\ \ln(K_{Te}C_e)$	B (J/mol)	16.58	17.63	18.52	19.66
		K_{Te}	1.351	1.317	1.310	1.324
		X^2	10.1	14.3	14.3	14.4
		R^2	0.9280	0.9312	0.9355	0.9279
Helsey	$\ln\ q_e = \left[\left(\frac{1}{n}\right)\ \ln\ K\right] - \left(\frac{1}{n}\right)\ \ln\ C_e$	K_{He}	2.721	2.980	3.457	2.874
		n	0.911	0.911	0.922	0.844
		X^2	28.2	26.3	29.7	30.6
		R^2	0.9456	0.9455	0.9791	0.9791
Dubinin-Radushkevich	$q_e = X'_m\ \exp(-K'\varepsilon^2)$	K'	6.108	5.971	5.412	5.018
		X'_m	6.979	8.239	9.272	10.913
		X^2	22.3	25.6	24.8	30.7
		R^2	0.9960	0.9981	0.9870	0.9799

3.7.4. The Halsey isotherm

The Halsey [34] adsorption isotherm can be given as

$$\ln\ q_e = \left[\left(\frac{1}{n}\right)\ \ln\ K\right] - \left(\frac{1}{n}\right)\ \ln\ C_e \tag{10}$$

This equation was suitable for multilayer adsorption. Especially, the fitting of this equation can be best used for heterotopous solids. $\ln q_e$ vs. $\ln 1/C_e$ Halsey adsorption isotherm is given in Fig. 10(C) and Table 3.

3.7.5. Dubinin-Radushkevich isotherm

The Dubinin-Radushkevich (D-R) equation was given as [35]:

$$q_e = X'_m\ \exp(-K'\varepsilon^2) \tag{11}$$

where q_e is the amount of MG dye adsorbed per unit mass of MWCNT-COOH adsorbent. X'_m is adsorption capacity. K' is a constant related to adsorption energy [35], is Polanyi potential and can be correlated as:

$$\varepsilon = RT\ \ln\left(1 + \frac{1}{C_e}\right) \tag{12}$$

R is the gas constant and T is adsorption temperature, K' gives the mean free energy E of adsorption per molecule of adsorbate when it is transferred to the surface of the solid from infinity in the solution and can be calculated using the following equation [35,38]:

$$E = \frac{1}{\sqrt{-2K'}} \tag{13}$$

The values of X'_m and K' were calculated from the intercept and slope of the $\ln\ q_e$ vs. ε^2 plots as shown in Fig. 10(D) and Table 3.

Also, comprised of experimental adsorption isotherms of Pb(II) ions by (a) GO, (b) GO-SH_1, (C) GO surface, and (D) G)-SH_3 surfaces as adsorbents. The equilibrium models used were the linear Langmuir (type I), Freundlich, Temkin, Helsey, and Dubinin-Radushkevich isotherm models. Initial concentration: 5–45 mg/L; adsorbent dosage: 20 mg; time: 60 min; and pH 6 and 298 K are shown in Fig. 11, and the comparison of adsorption capacities of various adsorbents for Pb(II) ion with other adsorbents is shown in Table 4.

3.8. Thermodynamic study

Temperature has a most important effluence on the adsorption capacity of adsorbent surface. Adsorption capacity of Pb(II) ion on GO, GO-SH_1, GO-SH_2, and

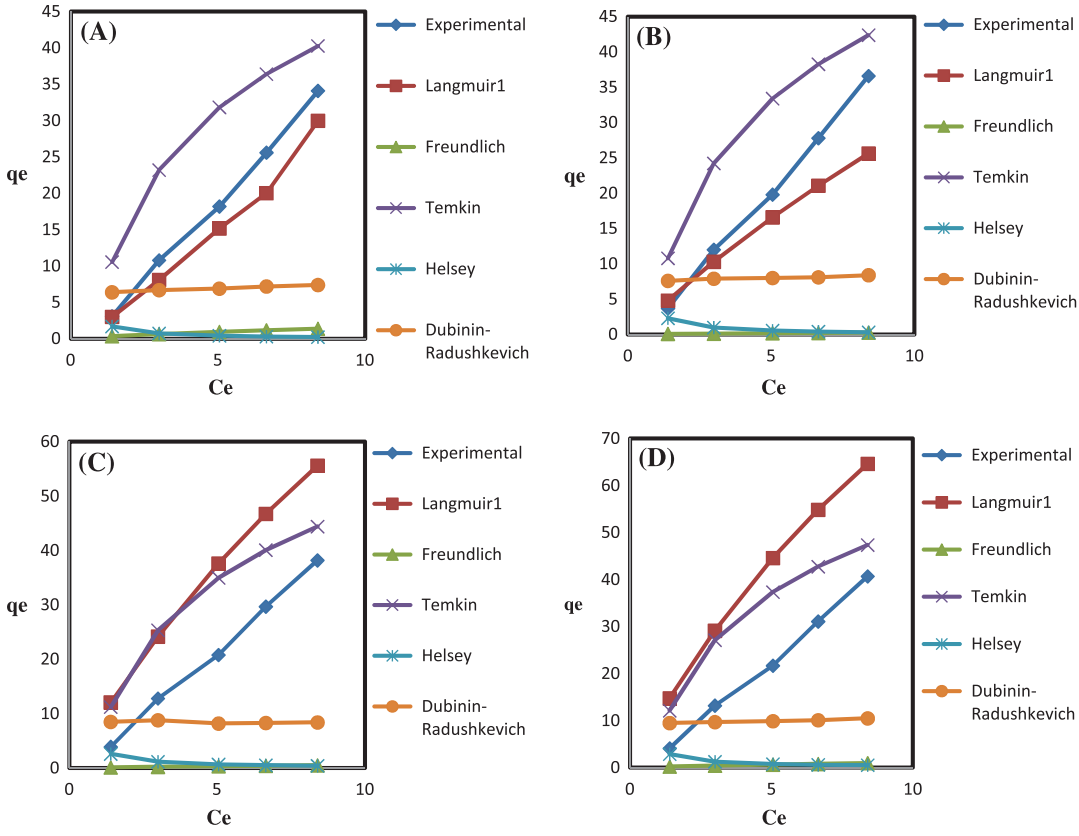

Fig. 11. Plot of adsorption density at equilibrium (q_e) vs. equilibrium concentration (C_e) for removal of Pb(II) ions by (A) GO surface, (B) GO-SH_1 surface, (C) GO-SH_2 surface, and (D) G-SH_3 surface. The equilibrium models used were the Langmuir (type I), Freundlich, Temkin, Helsey, and Dubinin–Radushkevich isotherm models. Initial concentration: 5–45 mg/L; adsorbent dosage: 20 mg; time: 60 min; and pH 6 and 298 K. For comparison between experimental results of adsorption of Pb(II) ion by GO, GO-SH_1, GO-SH_2, GO-SH_3 as surface adsorbents with Langmuir (type I), Freundlich, Temkin, Helsey, and Dubinin–Radushkevich isotherms.

GO-SH_3 surfaces was increased with increment in the temperature of solutions. This reveals that the adsorption of Pb(II) ion on GO, GO-SH_1, GO-SH_2, and GO-SH_3 surfaces was an endothermic process. The influential thermodynamic parameters, such as Gibbs free energy change of adsorption (ΔG°), enthalpy (ΔH°), and entropy (ΔS°), the adsorption of Pb(II) ion on GO, GO-SH_1, GO-SH_2, and GO-SH_3 surfaces was calculated to scrutiny the thermodynamic feasibility of the adsorption process and to confirm its nature using the following well-known equations [37]:

$$\Delta G = -RT \ \ln\left(K_{eq} = \frac{q_e}{C_e}\right) \tag{14}$$

$$\ln\left(K_{eq} = \frac{q_e}{C_e}\right) = \frac{\Delta S}{R} - \frac{\Delta H}{RT} \tag{15}$$

$$\Delta G^\circ = \Delta H^\circ - T\Delta S^{deg} \tag{16}$$

where T is the temperature in K, and R is the universal gas constant (8.314 J mol^{-1} K^{-1}). The Langmuir (type I) adsorption constant b was derived from the isotherm experiments. ΔH° and ΔS° can be obtained from the slope and intercept of the linear plots of ln (55.5b) vs. $1/T$, respectively. The data obtained were well fitted and in good agreement with type I adsorption isotherm model, which was later confirmed by the high R^2 values and low X^2 of the estimated thermodynamic parameters (Table 5). Fig. 12 shows linear plots of ln(55.5b) vs. $1/T$.

In the present study, the negative values of ΔG° indicated that adsorption of Pb(II) ion on GO, GO-SH_1, GO-SH_2, and GO-SH_3 surfaces was spontaneous in nature. The positive values of ΔH° indicated the adsorption of Pb(II) ion on GO, GO-SH_1, GO-SH_2, and GO-SH_3 surfaces was endothermic in nature. These results were concordance with subsection 3.5 and Fig. 6. Also, with the increase in temperatures, the values of the ΔG° were increased, which demonstrated that the

Table 4
Comparison of adsorption capacities of various adsorbents for Pb(II) ions

Adsorbent	q_e (mg/g)	Time	Temperature (K)	pH	Refs.
Magnetic $CoFe_2O_4$-reduced graphene oxide	299.4	120 (min)	298	5.3	[1]
Graphene oxide	111.1	60 (min)	298	6	This work
Carbon nanotube sheets	117.65	50 (min)	298	7	[5]
Carbon nanotubes	102.04	80–120 (min)	298	5	[10]
Thiol-functionalized cellulosic biomass	28.67	3 (h)	293	6	[10]
Amino modified multi-walled carbon nanotubes	58.26	90 (min)	318	6.2	[11]
Mesoporous carbon (OMC) with SBA-16	125.0	30 (min)	293	6	[22]
Poly2-hydroxyethyl methacrylate (PHEMA)	3.037	120 (min)	303	6	[25]
Copolymer 2-hydroxyethyl methacrylate with monomer methyl methacrylate P(MMA-HEMA)	31.447	120 (min)	303	6	[25]
Amino modified multi-walled carbon nanotubes	58.26	90 (min)	318	6.2	[37]
Manganese oxide-coated carbon nanotubes	78.74	2 (h)	298	5	[39]
Multi-walled carbon nanotubes	17.5	30 (min)	293	6	[23]
Functionalized graphene oxide-thiol (prepared with 60 mg cysteamine (GO-SH_1)	142.8	60 (min)	298	6	This work
Functionalized graphene oxide-thiol(prepared with 80 mg cysteamine (GO-SH_2)	200	60 (min)	298	6	This work
Functionalized graphene oxide-thiol(prepared with 100 mg cysteamine (GO-SH_3)	200	60 (min)	298	6	This work

Table 5
Thermodynamic functions of the removal of Pb(II) ions by the GO and GO-SHs adsorbents

		Functions		
Adsorbent	T (K)	ΔS° (kJ/mol K)	ΔH° (kJ/mol)	ΔG° (kJ/mol)
GO	288			−5.982
	298	0.099	22.70	−6.805
	308			−7.792
	318			−8.782
GO-SH1	288			−8.794
	298	0.199	48.75	−10.55
	308			−12.54
	318			−14.53
GO-SH2	288			−10.58
	298	0.203	54.77	−12.72
	308			−15.75
	318			−18.78
GO-SH3	288			−13.16
	298	0.298	72.70	−16.03
	308			−19.01
	318			−21.99

adsorption of Pb(II) ion on GO, GO-SH_1, GO-SH_2, and GO-SH_3 surfaces was an endothermic process. If the ΔH° value of adsorption process ranging is 40–800 kJ/mol, the adsorption is usually chemisorption, yet values less than 40 kJ/mol refer to a physisorption [38]. In this work, values of ΔH° were 22.70, 48.75, 54.77, and 72.77 (kJ/mol) from GO, GO-SH_1, GO-SH_2, and GO-SH_3 surfaces, respectively. So, these results may be demonstrated that adsorption Pb(II) ion on GO surface was a physisorption and adsorption Pb(II) ion

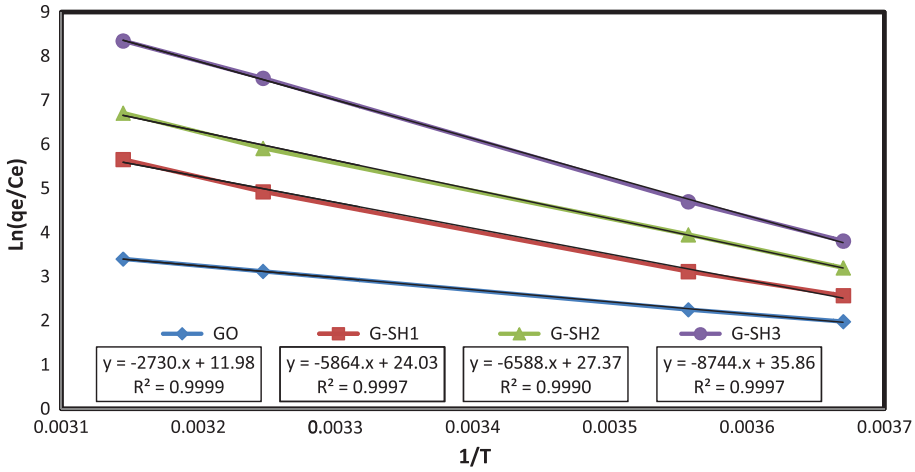

Fig. 12. Vant Hoff plot (the linear plot of $\ln(q_e/C_e)$ vs. $1/T$) for adsorption of Pb(II) ion by GO, GO-SH_1, GO-SH_2, and GO-SH_3 surfaces.

on GO-SH_1, GO-SH_2, and GO-SH_3 surfaces were chemisorption process. It is noticeable that the ΔG° values increased with rises in cysteamine concentration from 0 to 100 mg (GO to GO-SH_3) in adsorbents surfaces, which were −6.805, −10.55, −12.72, and −16.03 (kJ/mol) from GO, GO-SH_1, GO-SH_2, and GO-SH_3 surfaces, respectively, at temperature 298 (K), contact time 60 min, and pH [38–44].

It was found that free energy change for physisorption was generally between −20 and 0 kJ/ mol, the physisorption together with chemisorption within −20 to −80 kJ/mol, and pure chemisorption in the range of −80 to −400 kJ/mol [37].

4. Conclusion

In summary, the GO, GO-SH_1, GO-SH_2, and GO-SH_3 surfaces were used as efficient adsorbents for the rapid removal of Pb(II) ion from aqueous solutions. The effect of influential parameters such as contact time, initial Pb(II) ion concentration, pH, temperature, and cysteamine concentration was well investigated and optimized, and the optimized values are 60 min, 25 mg L^{-1}, 6, 298 K, and with the increase in cysteamine concentration, the adsorption Pb(II) ion on GO, GO-SH_1, GO-SH_2, and GO-SH_3 surfaces was increased. The results demonstrated that the adsorption of Pb(II) ion on GO, GO-SH_1, GO-SH_2, and GO-SH_3 surfaces was well fitted in good agreement with Langmuir isotherm model (Type I). Thermodynamic functions, such as ΔG°, ΔH°, and ΔS° were calculated and it reveals that the adsorption of Pb(II) ion on all the surfaces were spontaneous and endothermic in nature.

Acknowledgment

The author would like to thank the Islamic Azad, Islamshahr Branch for their financial support.

References

[1] Y. Zhang, L. Yan, W. Xu, X. Guo, L. Cui, L. Gao, Q. Wei, B. Du, Adsorption of Pb(II) and Hg(II) from aqueous solution using magnetic $CoFe_2O_4$-reduced graphene oxide, J. Mol. Liq. 191 (2014) 177–182.
[2] H. Mansoorian, A.H. Mahvi, A. Jonidi, Removal of lead and zinc from battery industry wastewater using electrocoagulation process, influence of direct and alternating current by using iron and stainless steel rod electrodes, Sep. Purif. Technol. 135 (2014) 165–175.
[3] D. Lin, X. Tian, T. Li, Z. Zhang, X. He, B. Xing, Surface-bound humic acid increased Pb^{2+} sorption on carbon nanotubes, Environ. Pollut. 167 (2012) 138–147.
[4] G.H. Safari, M. Zarrabi, M. Hosseini, H. Kamani, J. Jaafari, A.H. Mahvi, Trends of natural and acid-engineered pumice onto phosphorus ions in aquatic environment adsorbent preparation characterization and kinetic and equilibrium modeling, Desalin. Water Treat. 52 (2014) 1–13.
[5] B. Kakavandi, R. Rezaei Kalantary, M. Farzadkia, A.H. Mahvi, A. Esrafili, A. Azari, A.R. Yari, A.B. Javid, Enhanced chromium(VI) removal using activated carbon modified by zero valent iron and silver bimetallic nanoparticles, J. Environ. Health Sci. Eng. 12 (2014) 115.
[6] M. Tofighy, T. Mohammadi, Adsorption of divalent heavy metal ions from water using carbon nanotube sheets, J. Hazard. Mater. 185 (2011) 140–147.
[7] H. Yan, L. Yang, Z. Yang, H. Yang, A. Li, R. Cheng, Preparation of chitosan/poly(acrylic acid) magnetic composite microspheres and applications in the removal of copper(II) ions from aqueous solutions, J. Hazard. Mater. 229–230 (2012) 371–380.

[8] A.L.P.F. Caroni, C.R.M. de Lima, M.R. Pereira, J.L.C. Fonseca, Tetracycline adsorption on chitosan: A mechanistic description based on mass uptake and zeta potential measurements, Colloids Surf., B 100 (2012) 222–228.
[9] M. Auta, B.H. Hameed, Coalesced chitosan activated carbon composite for batch and fixed-bed adsorption of cationic and anionic dyes, Colloids Surf., B 105 (2013) 199–206.
[10] N. Kabbashi, M. Atieh, A. Al-Mamun, M. Mirghami, M. Alam, N. Yahya, Kinetic adsorption of application of carbon nanotubes for Pb(II) removal from aqueous solution, J. Environ. Sci. 21 (2009) 539–544.
[11] Z. Wu, Z. Cheng, W. Ma, Adsorption of Pb(II) from glucose solution on thiol-functionalized cellulosic biomass, Bioresour. Technol. 104 (2012) 807–809.
[12] H. Yan, X. Tao, Z. Yang, K. Li, H. Yang, A. Li, R. Cheng, Effects of the oxidation degree of graphene oxide on the adsorption of methylene blue, J. Hazard. Mater. 268 (2014) 191–198.
[13] Y. Li, Q. Du, T. Liu, X. Peng, J. Wang, J. Sun, Y. Wang, S. Wu, Z. Wang, Y. Xia, L. Xia, Comparative study of methylene blue dye adsorption onto activated carbon, graphene oxide, and carbon nanotubes, Chem. Eng. Res. Des. 91 (2013) 361–368.
[14] Y. Zhang, Y. Cheng, N. Chen, Y. Zhou, B. Li, W. Gu, X. Shi, Y. Xian, Recyclable removal of bisphenol A from aqueous solution by reduced graphene oxide–magnetic nanoparticles: Adsorption and desorption, J. Colloid Interface Sci. 421 (2014) 85–92.
[15] S. Wang, H. Sun, H.M. Ang, M.O. Tadé, Adsorptive remediation of environmental pollutants using novel graphene-based nanomaterials, Chem. Eng. J. 226 (2013) 336–347.
[16] N.M. Bandaru, N. Reta, H. Dalal, A.V. Ellis, J. Shapter, Enhanced adsorption of mercury ions on thiol derivatized single wall carbon nanotubes, J. Hazard. Mater. 261 (2013) 534–541.
[17] Y.J.O. Asencios, M.R. Sun-Kou, Synthesis of high-surface-area γ-Al_2O_3 from aluminum scrap and its use for the adsorption of metals: Pb(II), Cd(II) and Zn(II), Appl. Surf. Sci. 258 (2012) 10002–10011.
[18] G.D. Vuković, A.D. Marinković, S.D. Škapin, M. Ristić, R. Aleksić, A.A. Perić-Grujić, P.S. Uskoković, Removal of lead from water by amino modified multi-walled carbon nanotubes, Chem. Eng. J. 173 (2011) 855–865.
[19] O. Moradi, M. Norouzi, A. Fakhri, K. Naddafi, Interaction of removal ethidium bromide with carbon nanotube: Equilibrium and isotherm studies, J. Environ. Health Sci. Eng. 12(17) (2014) 1–9.
[20] A. Ahmadpour, N. Eftekhari, A. Ayati, Performance of MWCNTs and a low-cost adsorbent for chromium(VI) ion removal, J Nanostruct. Chem. 4(4) (2014) 171–178.
[21] P. Sharma, N. Hussain, D.J. Borah, M.R. Das, Kinetics and adsorption behavior of the methyl blue at the graphene oxide/reduced graphene oxide nanosheet−water interface: A comparative study, J. Chem. Eng. Data 58 (2013) 3477–3488.
[22] M. Anbia, S. Karami, Desulfurization of gasoline using novel mesoporous carbon adsorbents, J. Nanostruct. Chem. 5(1) (2015) 131–137.
[23] D.K. Venkata Ramana, J.S. Yu, K. Seshaiah, Silver nanoparticles deposited multiwalled carbon nanotubes for removal of Cu(II) and Cd(II) from water: Surface, kinetic, equilibrium, and thermal adsorption properties, Chem. Eng. J. 223 (2013) 806–815.
[24] T.K. Sen, S.P. Mahajan, K.C. Khilar, Adsorption of Cu^{2+} and Ni^{2+} on iron oxide and kaolin and its importance on Ni^{2+} transport in porous media, Colloids Surf., A 211 (2002) 91–102.
[25] O. Moradi, M. Aghaie, K. Zare, M. Monajjemi, H. Aghaie, The study of adsorption characteristics Cu^{2+} and Pb^{2+} ions onto PHEMA and P(MMA-HEMA) surfaces from aqueous single solution, J. Hazard. Mater. 170 (2009) 673–679.
[26] B. Erdem, A. Özcan, Ö. Gök, A.S. Özcan, Immobilization of 2,2′-dipyridyl onto bentonite and its adsorption behavior of copper(II) ions, J. Hazard. Mater. 163 (2009) 418–426.
[27] M. Anbia, S. Khoshbooei, Functionalized magnetic MCM-48 nanoporous silica by cyanuric chloride for removal of chlorophenol and bromophenol from aqueous media, J. Nanostruct. Chem. 5(1) (2015) 139–146.
[28] Y. Xue, H. Hou, S. Zhu, Competitive adsorption of copper(II), cadmium(II), lead(II) and zinc(II) onto basic oxygen furnace slag, J. Hazard. Mater. 162 (2009) 391–401.
[29] R.T. Yang, Adsorptions: Fundamental and Applications, John Wiley & Sons, Inc., New Jersey, NJ, 2003.
[30] L. Yan, Y. Li, L. Wang, Y. Zhang, X. Ma, Z. Ye, Preparation and adsorption performance of a novel bipolar PS-EDTA resin in aqueous phase, J. Hazard. Mater. 180 (2010) 98–105.
[31] F.M. Machado, C.P. Bergmann, T.H.M. Fernandes, E.C. Lima, B. Royer, T. Calvete, S.B. Fagan, Adsorption of reactive red M-2BE dye from water solutions by multi-walled carbon nanotubes and activated carbon, J. Hazard. Mater. 192 (2011) 1122–1131.
[32] H. Li, D. Xiao, H. He, R. Lin, P. Zuo, Adsorption behavior and adsorption mechanism of Cu(II) ions on amino-functionalized magnetic nanoparticles, Trans. Nonferrous Met. Soc. China 23 (2013) 2657–2665.
[33] X. Mi, G. Huang, W. Xie, W. Wang, Y. Liu, J. Gao, Preparation of graphene oxide aerogel and its adsorption for Cu^{2+} ions, Carbon 50 (2012) 4856–4864.
[34] M. Setareh Derakhshan, O. Moradi, The study of thermodynamics and kinetics methyl orange and malachite green by SWCNTs, SWCNT-COOH and SWCNT-NH_2 as adsorbents from aqueous solution, J. Ind. Eng. Chem. 20 (2014) 3186–3194.
[35] H. Li, Di Zhang, X. Han, B. Xing, Adsorption of antibiotic ciprofloxacin on carbon nanotubes: pH dependence and thermodynamics, Chemosphere 95 (2014) 150–155.
[36] H. Li, D. Zhang, X. Han, B. Xing, Adsorption of antibiotic ciprofloxacin on carbon nanotubes: pH dependence and thermodynamics, Chemosphere 95 (2014) 150–155.
[37] G.D. Vuković, A.D. Marinković, S.D. Škapin, M. Ristić, R. Aleksić, A. Perić-Grujić, P.S. Uskoković, Removal of lead from water by amino modified multi-walled carbon nanotubes, Chem. Eng. J. 173 (2011) 855–865.
[38] O. Moradi, K. Zare, M. Monajjemi, M. Yari, H. Aghaie, The studies of equilibrium and thermodynamic adsorption of Pb(II), Cd(II) and Cu(II) Ions from aqueous solution onto SWCNTs and SWCNT–COOH surfaces, Fullerenes, Nanotubes, Carbon Nanostruct. 18 (2010) 285–302.

[39] S.G. Wang, W.X. Gong, X.W. Liu, Y.W. Yao, B.Y. Gao, Q.Y. Yue, Removal of lead (II) from aqueous solution by adsorption onto manganese oxide-coated carbon nanotubes, Sep. Purif. Technol. 58 (2007) 17–23.
[40] A. Sarı, M. Tuzen, M. Soylak, Adsorption of Pb(II) and Cr(III) from aqueous solution on Celtek clay, J. Hazard. Mater. 144 (2007) 41–46.
[41] A. Sarı, M. Tuzen, Kinetic and equilibrium studies of Pb(II) and Cd(II) removal from aqueous solution onto colemanite ore waste, Desalination 249 (2009) 260–266.
[42] A. Sarı, M. Tuzen, De. Cıtak, M. Soylak, Adsorption characteristics of Cu(II) and Pb(II) onto expanded perlite from aqueous solution, J. Hazard. Mater. 148 (2007) 387–394.
[43] A. Sarı, D. Çıtak, M. Tuzen, Equilibrium, thermodynamic and kinetic studies on adsorption of Sb(III) from aqueous solution using low-cost natural diatomite, Chem. Eng. J. 162 (2010) 521–527.
[44] A. Sarı, M. Tuzen, Removal of Cr(VI) from aqueous solution by Turkish vermiculite: Equilibrium, thermodynamic and kinetic studies, Sep. Sci. Technol. 43 (2008) 3563–3581.